Nuclear Instruments and Methods in Physics Research A 608 (2009) 107–115

Contents lists available at ScienceDirect

Nuclear Instruments and Methods in Physics Research A

journal homepage: www.elsevier.com/locate/nima

$MgWO_4$–A new crystal scintillator

F.A. Danevich [a,*], D.M. Chernyak [a], A.M. Dubovik [b], B.V. Grinyov [b], S. Henry [c], H. Kraus [c], V.M. Kudovbenko [a], V.B. Mikhailik [c], L.L. Nagornaya [b], R.B. Podviyanuk [a], O.G. Polischuk [a], I.A. Tupitsyna [b], Yu.Ya. Vostretsov [b]

[a] Institute for Nuclear Research, MSP 03680 Kyiv, Ukraine
[b] Institute for Scintillation Materials , 61001 Kharkiv, Ukraine
[c] University of Oxford, Department of Physics, Keble Road, Oxford OX1 3RH, UK

ARTICLE INFO

Article history:
Received 15 April 2009
Received in revised form
13 June 2009
Accepted 16 June 2009
Available online 25 June 2009

Keywords:
$MgWO_4$ crystal
Scintillation detector
Cryogenic scintillator

ABSTRACT

Magnesium tungstate ($MgWO_4$) crystals of ~1 cm^3 volume were obtained for the first time using a flux growth technique. The crystal was subjected to comprehensive characterisation that included room-temperature measurements of the transmittance, X-ray luminescence spectra, afterglow under X-ray excitation, relative photoelectron output, energy resolution, non-proportionality of scintillation response to γ-quanta, response to α-particles, and pulse shape for γ-quanta and α-particles. The light output and decay kinetics of $MgWO_4$ were studied over the temperature range 7–305 K. Under X-ray excitation the crystal exhibits an intense luminescence band peaking at a wavelength of 470 nm; the intensity of afterglow after 20 ms is 0.035%. An energy resolution of 9.1% for 662 keV γ-quanta of ^{137}Cs was measured with a small (≈0.9 g) sample of the $MgWO_4$ crystal. The photoelectron output of the $MgWO_4$ crystal scintillator is 35% that of $CdWO_4$ and 27% that of NaI(Tl). The detector showed pulse-shape discrimination ability in measurements with α-particles and γ-quanta, which enabled us to assess the radioactive contamination of the scintillator. The results of these studies demonstrate the prospect of this material for a variety of scintillation applications, including rare event searches.

1. Introduction

Scintillators are widely used for various applications where the detection of ionising radiation and particles is required. Despite the relatively long history of research there has always been interest in new scintillators. There is no single scintillation material suitable for all applications and the intention is now to tailor the performance characteristics of the scintillators for specific applications. The introduction of lead tungstate as a scintillation detector for high-energy physics is an excellent example of when the best performance is achieved by a compromise between a few characteristics, i.e. scintillation efficiency, response time, stopping power and radiation hardness. Similarly, the need for fast detectors with high light output for medical imaging has motivated the development of several Ce-doped scintillators over the last few decades.

The search and characterisation of new materials is also driven by new developments in science. A new field of application, which has emerged recently, is the next generation of cryogenic scintillation detectors for particle physics experiments, which require powerful background discrimination combined with excellent energy threshold and resolution [1]. These detectors allow the discrimination between electrons, α-particles, and nuclear recoils. They are becoming indispensable tools for experiments searching for rare events such as interactions with weak interacting massive particles (WIMPs, particles predicted by the Supersymmetry models, possible component of dark matter in the universe), neutrinoless ββ-decay or radioactive decay of long-lived nuclei [2–4]. As there are many materials that scintillate at cryogenic temperatures, the technology allows us to choose the most appropriate material for each specific experimental objective. Therefore it is important to test different materials of interest in the same experimental environment. While experiments searching for ββ-decays and studying rare decay processes require certain elements in a detector, dark matter searches, for instance the EURECA project [5], will require a variety of scintillation targets to verify the nature of a detected signal.

Magnesium Tungstate ($MgWO_4$) is of particular interest to such experiments due to the combination of heavy (W) and light (Mg and O) elements. WIMPs are expected to scatter predominantly on the tungsten nucleus. The most stringent dark matter limit can be set, therefore, by selecting only tungsten recoils. Carrying out this selection requires knowledge of the quenching factor—the ratio of the light output for an electron to the light output for a nuclear recoil. The quenching factor decreases with increasing atomic mass; hence so a better separation between

* Corresponding author. Tel.: +380 44 525 1111; fax: +380 44 525 4463.
E-mail address: danevich@kinr.kiev.ua (F.A. Danevich).

0168-9002/$ - see front matter © 2008 Elsevier B.V. All rights reserved.
doi:10.1016/j.nima.2009.06.040

species of recoiling nucleus could be achieved in $MgWO_4$, where the tungsten is accompanied only by much lighter elements than (for example) in $ZnWO_4$.

Rare event searches, operating at low temperatures, have an important advantage over mainstream scintillator applications as the intrinsic luminescence light yield usually increases with cooling. With cooling, also the time constants for the scintillation process increase, but this is not a significant problem in rare event searches. Many materials have already been investigated and quite a few are promising [6]. Recent studies of magnesium tungstate have demonstrated that this compound could be an attractive scintillation material for a cryogenic rare event search [7]. This compound has long been known as an efficient green phosphor [8], but it has never been characterised as a scintillator owing to a lack of single-crystalline samples.

The aim of this work was to develop single $MgWO_4$ crystals and to study their optical, luminescence, and scintillation properties. Some preliminary results of these investigations were reported in [9]. We have studied the following properties of $MgWO_4$ for the first time: response to α-particles; pulse-shape discrimination between α-particles and γ-quanta, afterglow, non-proportionality of light output, temperature dependence of scintillation output, decay kinetics down to a temperature of 7 K; and the radioactive contamination.

2. $MgWO_4$ crystal

Due to its high-temperature phase transition, $MgWO_4$ cannot be grown using the conventional Czochralski method. The technology for flux growth has been developed at the Institute for Scintillation Materials (Kharkiv, Ukraine). A stoichiometric mixture of MgO and WO_3 (99.99%) was added to the flux prepared from Na_2WO_4 (99.95%) at 790 °C in a platinum crucible. Single-crystalline samples of $MgWO_4$ crystals of ca. 1 cm^3 were grown by pulling the seed from the melted flux solution (see Fig. 1). The main characteristics of $MgWO_4$ crystal scintillators are listed in Table 1.

$MgWO_4$ is a biaxial crystal with high refractive index and clear birefringence [10]. Monoclinic β-$MgWO_4$ experiences a phase transition at 1165 °C into high-temperature α-$MgWO_4$ with triclinic structure [13,14]. The crystalline structure of $MgWO_4$ has been studied in several works [15–19].

Fig. 1. Produced $MgWO_4$ single crystal. The scale is in centimeters.

3. Results and discussion

3.1. Transmittance, luminescence and afterglow for X-ray excitation

The transmittance of a $MgWO_4$ crystal of 1.1 mm thickness was measured in the spectral range 300–700 nm using a Perkin Elmer lambda 15 spectrophotometer. The transmission curve is shown in Fig. 2. We infer that the strong absorption in the region of 320–420 nm, which causes the yellowish coloration of the sample, is due to the impurities or defects in the crystal. The use of the flux technique implies that the components of the flux can form ubiquitous defects and impurity centres in the crystals. Furthermore, since the flux was of lower purity than other components used for crystal production, this appears to have contributed to the total level of impurities in the crystal. Further purification of the initial raw compounds, especially the flux, should help to improve the optical properties of the crystal.

Nevertheless, even with the current absorption, large-volume $MgWO_4$ crystals are expected to exhibit a reasonable transparency in the region of intrinsic emission. The emission spectrum of the $MgWO_4$ crystal was measured under X-ray excitation at room-temperature, using a spectrophotometer KSVU-23 equipped with

Table 1
Properties of $MgWO_4$ crystal scintillators.

Density	5.66 g cm^{-3}	[10]
Melting point	1358 °C	[11]
Structural type	Wolframite-type monoclinic	[12]
Space group	P2/c	[12]
Cleavage plane	(0 1 0)	Present work
Hardness (Mohs)	4.5	[10]
Emission maximum	470 nm	Present work
Decay time[a]	36 μs	Present work
Photoelectron output[b]	35% of $CdWO_4$ 27% of NaI(Tl)	Present work

[a] For γ rays, at room temperature.
[b] For γ rays, at room temperature. The energy spectra to estimate relative photoelectron output were obtained off-line by calculating the area of each pulse from its start up to 80 μs.

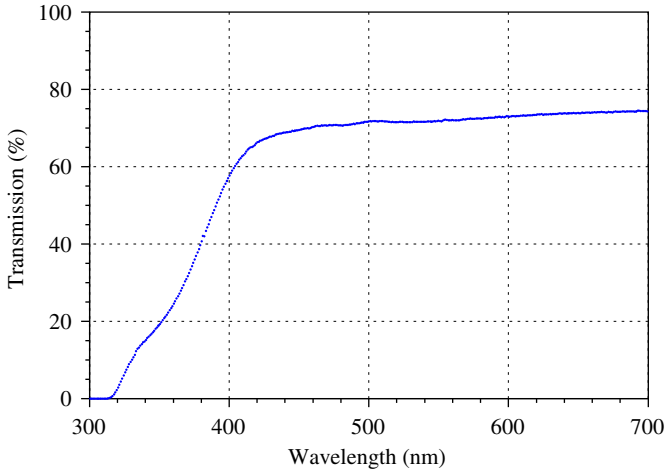

Fig. 2. Optical transmission curve of $MgWO_4$ crystal.

a REIS-I X-ray source (Ag anode, $U = 35$ kV, $I = 0.1$ mA). The crystal shows intense luminescence at a maximum of 470 nm (see Fig. 3). This agrees well with the room temperature data obtained for a powder sample [7]. The emission spectrum of $MgWO_4$ is similar to other tungstates having the wolframite structural type, e.g. $CdWO_4$ and $ZnWO_4$.

Measurements of the afterglow were carried out using a dedicated setup for studies of the kinetic characteristics of scintillators. A sample of $MgWO_4$ crystal 1 mm thick, installed at the distance 3 cm from the X-ray tube, was excited by X-ray pulse emitted by a RAPAN-200 X-ray source ($U = 120$ kV, $I = 3$ mA) with a duration of 2 s. The measurements were carried out in transmission geometry. The level of afterglow measured 20 ms after termination of excitation was 0.035%, which is comparable with BGO, $CdWO_4$, $ZnWO_4$ and substantially lower than that of the commonly used NaI(Tl) and CsI(Tl) having the afterglow on the level of 0.5–5%.

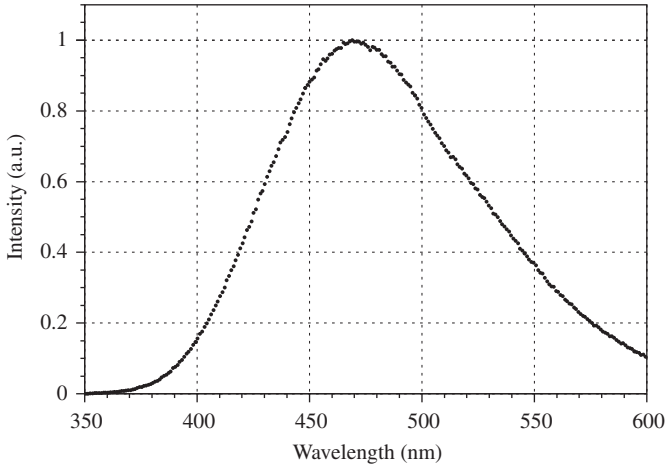

Fig. 3. Emission spectra of $MgWO_4$ crystal excited by X-rays.

3.2. Response of $MgWO_4$ crystal scintillator to γ-quanta

To study the scintillation properties, we used a 0.87 g sample of a $MgWO_4$ crystal in the shape of an oval cylinder with axes 5.9, 8.7 and 3.2 mm. The crystal was coupled to a 3″ Philips XP2412 photomultiplier (PMT) with a bi-alkali photocathode, using a Dow Corning Q2-3067 optical couplant. The crystal was surrounded by a reflecting cup $\varnothing 20\,\text{mm} \times 20\,\text{mm}$, made of dielectric mirror foil from 3 M [20], having specular reflectivity 98% in the visible region. The crystal was irradiated with γ-quanta from ^{137}Cs, ^{207}Bi, ^{133}Ba, and ^{241}Am γ-sources. Taking into account the long decay time of $MgWO_4$ (see Section 3.5), the PMT signals were accumulated using a 20 MS/s transient digitizer based on a 12-bit ADC (AD9022). The energy spectra were obtained off-line by calculating the area of each pulse from its start up to 80 μs.

Fig. 4 shows the pulse amplitude spectra measured for the $MgWO_4$ scintillator with γ and X-ray sources. The energy resolution for the 662 keV γ-line of ^{137}Cs was found to be 9.1%.

Fig. 5 shows the energy resolution of the $MgWO_4$ crystal scintillator measured over the 17–1064 keV energy range. The

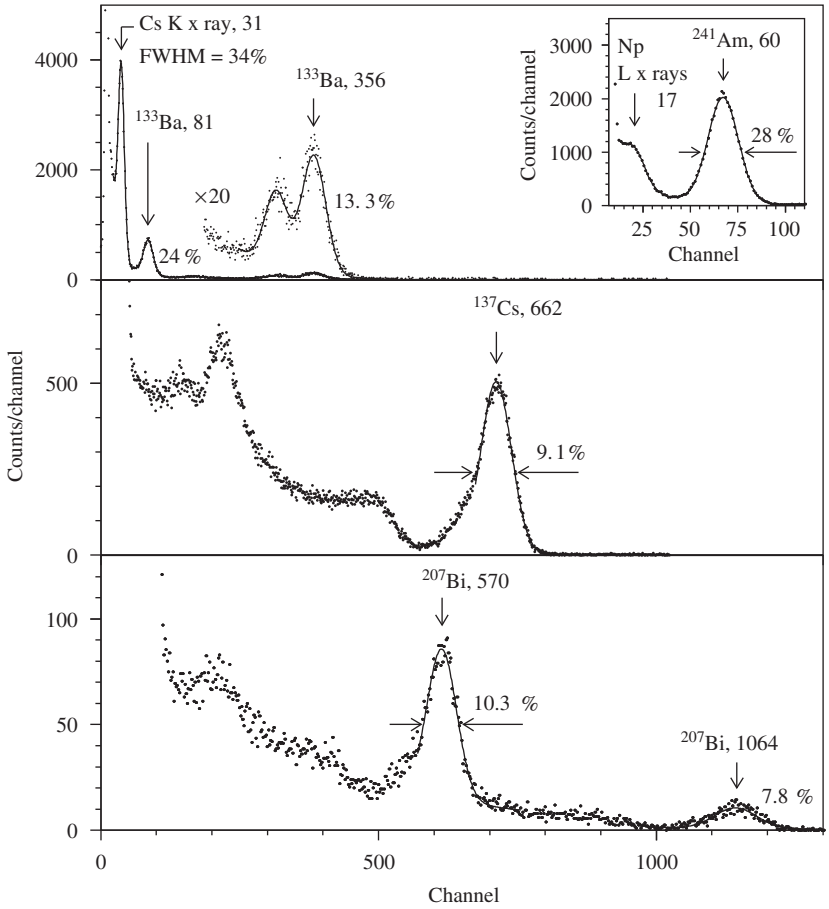

Fig. 4. Energy spectra of ^{133}Ba, ^{241}Am (inset), ^{137}Cs, and ^{207}Bi γ-rays measured for the $MgWO_4$ scintillation crystal. Fits of the γ-peaks are shown as solid lines. Energies of the γ and X-ray lines are in keV.

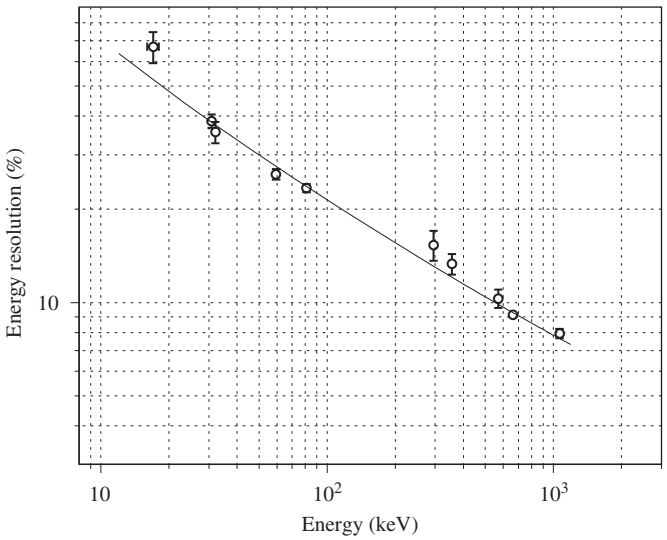

Fig. 5. Energy resolution (FWHM) vs. γ-energy, measured with the $MgWO_4$ crystal scintillator.

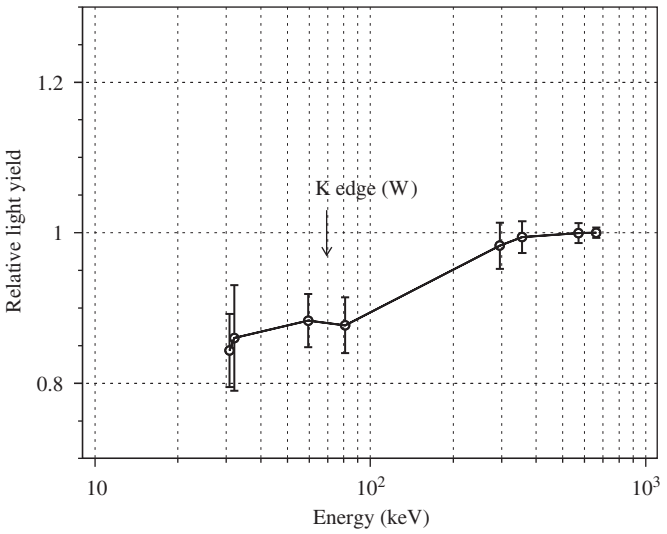

Fig. 7. Non-proportionality of the scintillation response for $MgWO_4$.

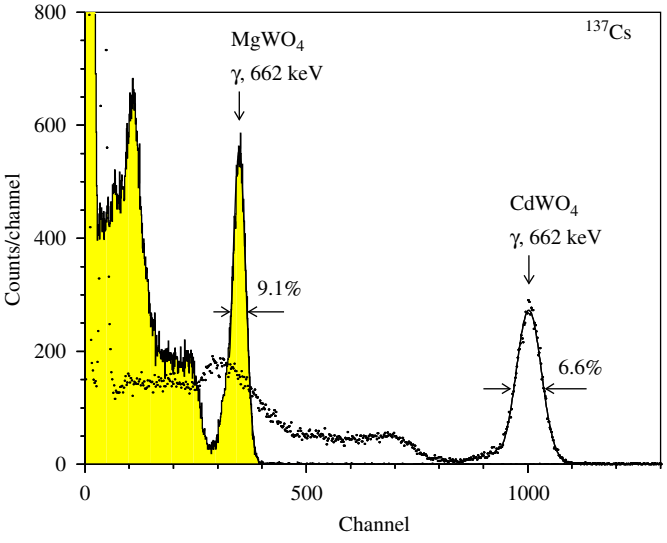

Fig. 6. Energy spectra of 662 keV ^{137}Cs γ-rays measured for $MgWO_4$ and $CdWO_4$ scintillation crystals. Fits of the γ-peaks are shown as solid lines.

data were fitted with the help of the chi-square method (χ^2/n.d.f. = 13.15/8 = 1.64, where n.d.f. is number of degrees of freedom) by the function FWHM (%) = a+$(b \times E_\gamma)^{1/2}/E_\gamma$ (where E_γ is the energy of γ and X-ray quanta in keV) with parameters $a = 1.6 \pm 3$ and $b = (3.86 \pm 0.24) \times 10^4$ keV. The energy resolution obtained with the first sample of $MgWO_4$ is comparable to characteristic of GSO, $ZnWO_4$, BGO and BaF_2 crystal scintillators (FWHM ≈9–12%). At the same time it is still far from the scintillation materials, like NaI(Tl), CsI(Tl), $CdWO_4$, CaF_2(Eu) (FWHM ≈6–8%), not to mention recently developed $LaCl_3$(Ce), $LaBr_3$(Ce), LSO showing the energy resolution up to 3–5% for a 662 keV γ line of ^{137}Cs.

The photoelectron output of the detector with the $MgWO_4$ crystal was found to be 35% relative to a $CdWO_4$ scintillator ($10 \times 10 \times 2$ mm^3) (see Fig. 6), and 27% relative to a NaI(Tl) scintillator (∅40 mm × 40 mm). To estimate light yield of the scintillator in photons per MeV, we have calculated the quantum efficiency of the PMT (QE) with respect to the $MgWO_4$ and NaI(Tl) emission spectra. We have obtained $QE_{MgWO_4} = 0.14$ and $QE_{NaI(Tl)} = 0.20$ using the emission spectrum of $MgWO_4$ (Fig. 3), NaI(Tl) [21], and specification of the PMT XP2412 photocathode [22]. Assuming the light yield of NaI(Tl) 38×10^3 photons per MeV [21], and the equal light collection from the scintillators, we have obtained the light yield of $MgWO_4$ scintillator to be on the level of $\approx 15 \times 10^3$ photons per MeV. This value is just a rough estimation, taking into account the rather low accuracy of our assumption concerning the light collection.

3.3. Non-proportionality of scintillation response

We studied the non-proportionality of the scintillation response of the $MgWO_4$ scintillator using the same experimental set-up as for the measurements described in Subsection 3.2. Gamma and X-ray quanta from ^{241}Am (17 and 59.5 keV), ^{137}Cs (32.1 and 661.7 keV), ^{133}Ba (30.9, 81.0, 295.3 and 356.0 keV), and ^{207}Bi (569.7 keV) sources were used in these measurements. The measured relative light output per deposited energy, compared with that of the 661.7 keV γ-line (^{137}Cs), is displayed in Fig. 7, showing a noticeable decrease towards lower energies. The dependence is similar to that observed for $CdWO_4$ [23–25], $CaWO_4$ [26] and $ZnWO_4$ [27] scintillators, as well as for most inorganic scintillators [28–30].

3.4. Response to α-particles

The α/β ratio was measured with the $MgWO_4$ crystal using collimated α-particles from a ^{241}Am source. The opening of the polytetrafluoroethylene collimator was ∅0.75 mm × 2 mm. The energy of the α-particles after the collimator was shown (using a surface-barrier detector) to reduce to about 5.25 MeV after 2 mm of air. The energy scale of the detector was measured with γ-quanta from a ^{207}Bi source. To prevent changes in the light collection potentially caused by reconfiguring the set-up, the measurements with γ-quanta were carried out while the ^{241}Am α-source remained installed in the set-up. Fig. 8 shows the energy spectrum of the α-particles measured with the $MgWO_4$ scintillator. The α/β ratio is 0.186(2) for 5.25 MeV α-particles. The direction of the α-particles was parallel to the crystal axis [1 0 0].

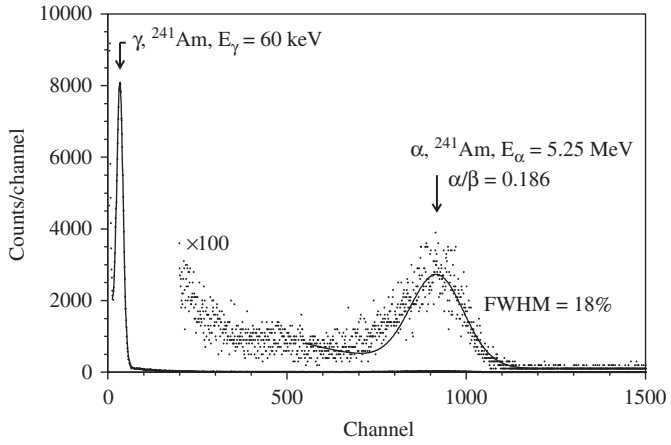

Fig. 8. The energy spectrum measured with 5.25 MeV α-particles from an ^{241}Am source (dots), in the direction parallel to the crystal axis [1 0 0]. A fit of the γ and α-peaks with a Gaussian is shown as a solid line.

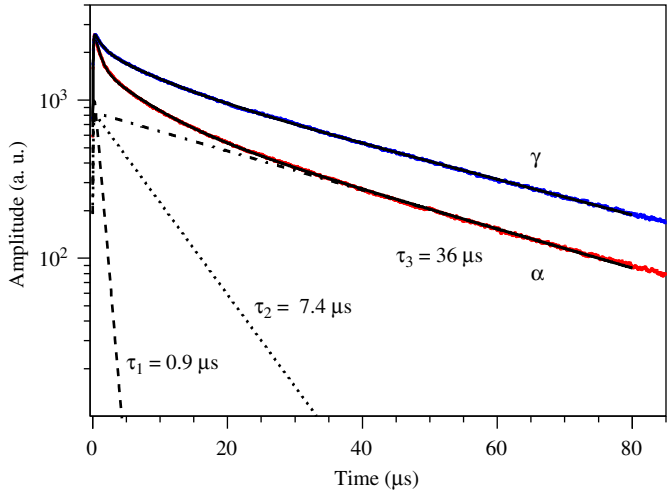

Fig. 9. Scintillation decay curves in $MgWO_4$ crystal measured for γ- and α-excitations at 291 K. Three components of scintillation signal for α-particles with decay times of 0.9, 7.4 and 36 μs are shown. Fitting functions for γ- and α-pulses are shown by solid lines.

The α/β ratio was also measured for two other directions using a collimated α-beam parallel to the [0 0 1] and [0 1 0] crystal axes. This gave $\alpha/\beta = 0.164(3)$ in the direction [0 0 1] and $\alpha/\beta = 0.195(3)$ in the direction [0 1 0]. A dependence of the α/β ratio on the direction of α-irradiation relative to crystal axes has also been observed in other crystal scintillators with wolframite structure, i.e. $CdWO_4$ [31] and $ZnWO_4$ [32], this is due to the considerable anisotropy. This effect contributes to the deterioration of the energy resolution for α-particles emitted by radioactive impurities, captured inside a scintillation crystal.

3.5. Decay kinetic for γ-rays and α-particles

The pulse shapes of the $MgWO_4$ scintillator were studied with the 12-bit, 20 MS/s transient digitizer, using the collimated ^{241}Am source to generate α-particles, and a ^{60}Co source for γ-quanta. The measurements were carried out at a temperature of 291 ± 1 K.

The shape of the light pulses produced by α-particles and γ-rays is shown in Fig. 9. To obtain the pulse shapes, a few thousand individual α (γ) events with amplitudes corresponding to the α-peak of ^{241}Am were summed. The pulses were fitted by the function

$$f(t) = \sum A_i[\exp(-t/\tau_i) - \exp(-t/\tau_0)]/(\tau_i - \tau_0), \quad (1)$$

where A_i are the relative intensities, τ_i are the decay constants for different light-emission components, and τ_0 the integration constant of the electronics ($\tau_0 = 0.09$ μs). Three decay components were observed with $\tau_1 \approx 1$ μs, $\tau_2 \approx 7$–10 μs and $\tau_3 \approx 36$–40 μs with different intensities for γ-rays and α-particles (see Fig. 9 and Table 2).

As one can see, $MgWO_4$ is a rather slow scintillator in comparison to widely used scintillation materials having decay times in the range from a few to tens of nanoseconds (liquid and plastic scintillators, $PbWO_4$, LSO and organic crystals), fractions of microsecond ($LaBr_3$(Ce), $LaCl_3$(Ce), GSO, BGO and NaI(Tl)), and microseconds (CaF_2(Eu), CsI(Tl)). At the same time the decay kinetic of $MgWO_4$ is comparable to well-known $CaWO_4$, $CdWO_4$ and $ZnWO_4$ crystal scintillators having the decay time more than 10 μs . However, the slow decay time is acceptable for applications (like dark matter experiments) where very rare counting rate is expected.

3.6. Pulse-shape discrimination between γ-rays and α-particles

The difference in pulse shapes allows us to discriminate γ (β) events from those induced by α-particles. This was done using the optimal filter method proposed in [33], and successfully used for $CdWO_4$ [34] and several other crystal scintillators. The shape indicator (SI) – a numerical characteristic – was calculated for each scintillation event produced by $MgWO_4$ as follows:

$$SI = \sum f(t_k)P(t_k) / \sum f(t_k), \quad (2)$$

where the sum is over time channels k from the origin of the pulse up to 80 μs; $f(t_k)$ is the digitized amplitude of the signal (at the time t_k). The weight function $P(t_k)$ is defined as

$$P(t) = [f_\alpha(t) - f_\gamma(t)]/[f_\alpha(t) + f_\gamma(t)], \quad (3)$$

where $f_\alpha(t)$ and $f_\gamma(t)$ are the reference pulse shapes for α-particles and γ-quanta.

Using this approach we achieved a clear discrimination between α-particles and γ-rays. This is illustrated in Fig. 10, which shows the shape indicator distributions measured with the $MgWO_4$ crystal for α-particles ($E_\alpha \approx 5.25$ MeV) and γ-quanta (≈ 1 MeV). The figure of merit (FOM) – a measure of discrimination ability – is calculated using the following expression:

$$\mathrm{FOM} = |SI_\alpha - SI_\gamma|/(\sigma_\alpha^2 + \sigma_\gamma^2)^{1/2}, \quad (4)$$

where SI_α and SI_γ are mean SI values for the distributions of α-particles and γ-quanta, and σ_α and σ_γ are the standard deviations of the Gaussian distributions. For the data presented in Fig. 10, the figure of merit is 5.2.

It should be mentioned that the optimal filter method allows us to detect the difference in the pulse shape when the crystal is irradiated by α-particles in different directions with respect to the crystal axes. The difference is visible in the shape indicator distributions. The mean value of SI_α for a particle impinging on the crystal along the [1 0 0] crystal axis is 154.3 ± 0.3, while the shape indicator distributions have slightly shifted maxima at $SI_\alpha = 148.7 \pm 0.4$ (irradiation along [0 0 1]) and $SI_\alpha = 140.9 \pm 0.4$ (irradiation along [0 1 0]). Such directional variation of SI_α was also noticeable for $CdWO_4$ [31] and $ZnWO_4$ [32] crystal scintillators.

Table 2
Decay times for the $MgWO_4$ scintillator for γ-quanta and α-particles (irradiation along the [1 0 0] crystal axis) at 291 K.

Type of irradiation	Decay constants and relative intensities		
	τ_1 (A_1)	τ_2 (A_2)	τ_3 (A_3)
γ rays	1.4±0.2 μs (1.4±0.3%)	9.7±1.8 μs (10±2%)	40±2 μs (88.6±2.4%)
α particles	0.9±0.2 μs (3±0.3%)	7.4±0.9 μs (16±2%)	36±2 μs (81±2%)

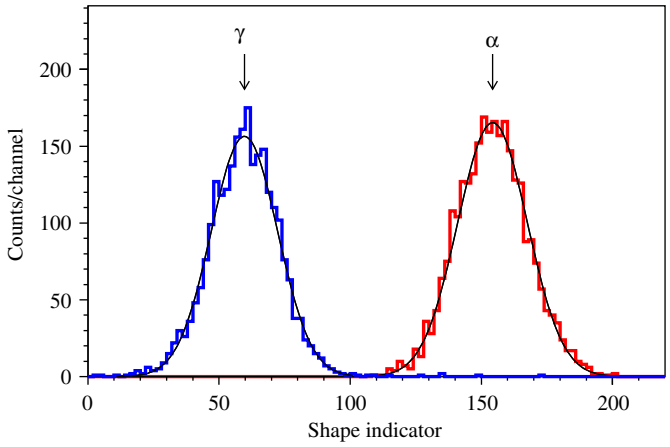

Fig. 10. The shape indicator (see text) distributions measured for $MgWO_4$ scintillator irradiated by α-particles ($E_\alpha \approx 5.3$ MeV) and γ-quanta (≈1 MeV). The distributions were fitted by Gaussian functions (solid lines).

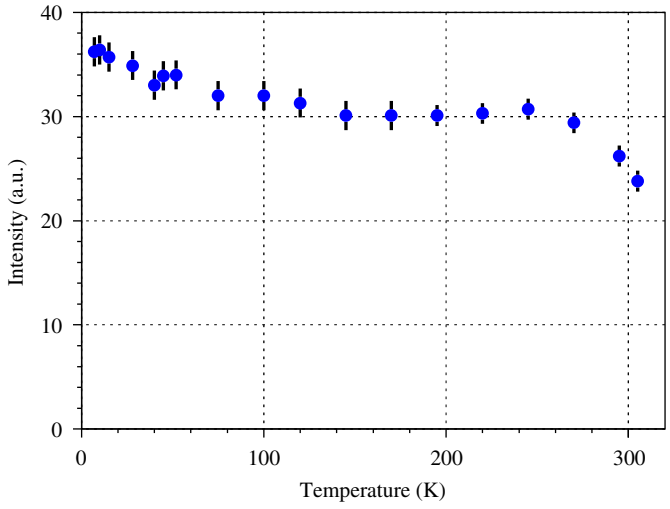

Fig. 11. Temperature dependence of the light output of the $MgWO_4$ crystal scintillator for excitation with ^{241}Am α-particles.

3.7. Low-temperature measurements of light output and decay time

The relative scintillation intensity and decay kinetics of $MgWO_4$ were studied over the temperature range 7–305 K, for a sample of the crystal of oval shape 8.3 × 5.8 × 1.1 mm^3, placed in a He-flow optical cryostat and excited with ^{241}Am α-particles. The measurements of scintillation light were carried out using a green-sensitive photomultiplier (Electron Tubes 9124A) and using the multiple photon counting technique [35].

The variation with temperature of the light output of $MgWO_4$ in the temperature interval 7–305 K is shown in Fig. 11. The relative scintillation efficiency is found to be 33±12% that of $ZnWO_4$ at $T = 7$ K. It should be noted that this is substantially lower than the ratio of the light output for the powder samples, which was measured to be 90±15% [7]. This can be readily explained by the inferior quality of the $MgWO_4$ crystal compared to the $ZnWO_4$ scintillator. This demonstrates that there is a significant scope for improving the performance of $MgWO_4$ as a scintillator.

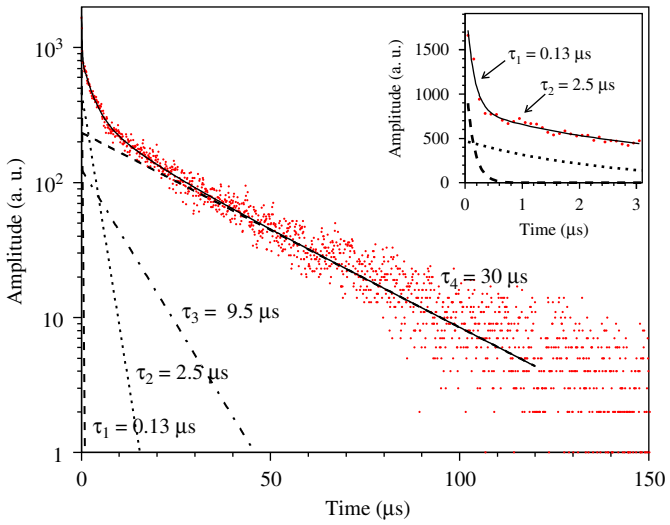

Fig. 12. Decay of scintillation in the $MgWO_4$ crystal, measured for α-particles from a ^{241}Am source, using the multiple photon counting technique at $T = 305$ K. Four components with time decays of 0.13, 2.5, 9.5 and 30 μs are displayed as straight lines. The fitting function of the pulse shape is shown by a solid line. Inset shows a first part of the pulse.

Fig. 12 shows the scintillation pulse shape of the $MgWO_4$ crystal measured at 305 K. To obtain the best fit of the experimental data we used a sum of four exponential functions with the following decay time constants: $\tau_1 = 0.13$ μs, $\tau_2 = 2.5$ μs, $\tau_3 = 9.5$ μs, and $\tau_4 = 30$ μs. It should be noted that the fastest ($\tau_1 \approx 0.1$–0.2 μs) decay component of the scintillation signal was not resolved in the measurements with the transient digitizer (see Subsection 3.5) due to its lower time resolution.

The longest decay time constant slowly increases as the temperature falls to 30 K and then rapidly increases with further cooling as shown in Fig. 13. This is a characteristic feature of the decay process of tungstates, caused by the competition of the radiative and non-radiative transitions within the emission centre, which constitutes a metastable level just below the emitting one [36,37]. At $T = 7$ K the decay time constants are found to be as follows: $\tau_1 = 1.1$ μs, $\tau_2 = 6$ μs, $\tau_3 = 20$ μs and $\tau_4 = 94$ μs.

3.8. Low-background measurements

The radioactive contamination of the $MgWO_4$ crystal was tested in the low-background set-up at the Institute for Nuclear

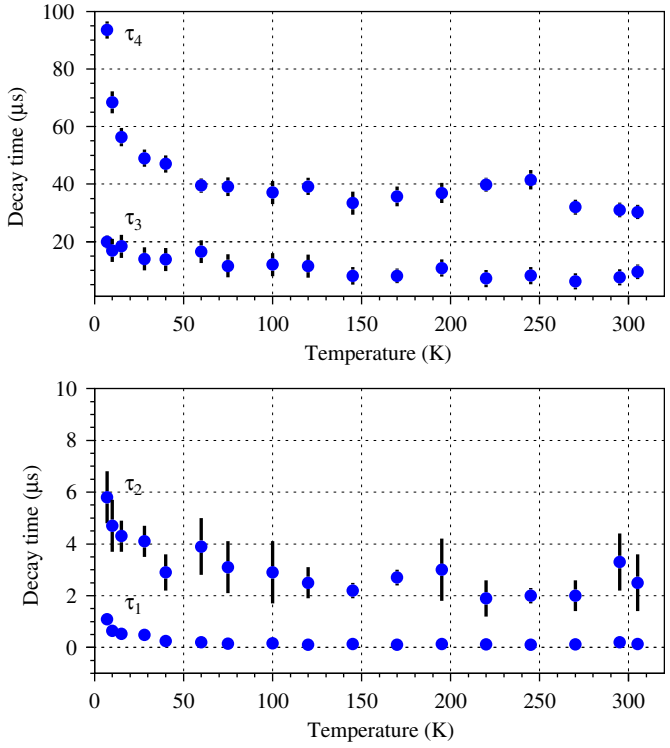

Fig. 13. Temperature dependence of the decay time constants of $MgWO_4$ (^{241}Am α-source).

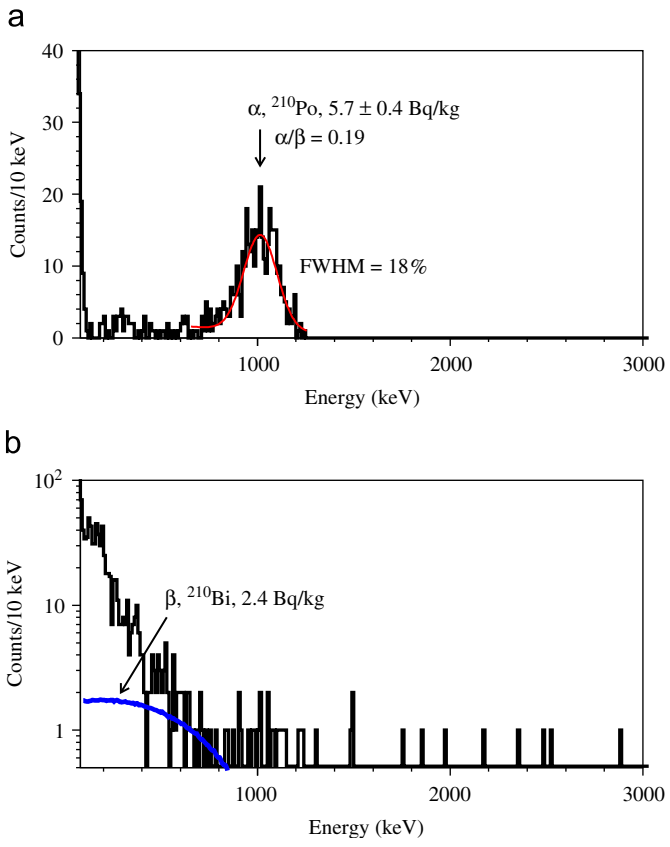

Fig. 14. Energy spectra of $MgWO_4$ scintillator (0.83 g) measured in the low-background set-up over 17 h and selected by pulse-shape discrimination. (a) The energy spectra of α-events. The fit of the ^{210}Po peak is shown as the solid line. (b) The energy spectrum of γ(β) events. The distribution of ^{210}Bi events, corresponding to an activity of 2.4 Bq kg^{-1}, excluded at 90% C.L., is shown as a solid line.

Table 3
Radioactive contamination of the $MgWO_4$ crystal. Upper limits are given for $k = 1.645$ (or 90% C.L.).

Chain	Source	Activity (Bq kg^{-1})
^{232}Th	^{232}Th	<0.28
	^{228}Th	<0.05
^{238}U	^{226}Ra	<0.05
	^{210}Pb	<2.4
	^{210}Po	5.7 ± 0.4
	^{40}K	<1.6
	^{90}Sr–^{90}Y	<1.5
	^{147}Sm	<0.54

Research (Kyiv, Ukraine). In the set-up, the scintillating crystal, covered by 3 layers of polytetrafluoroethylene tape, was viewed by a 3″ photomultiplier tube (Philips XP2412) through a high-purity polystyrene light guide (∅66 × 111 mm). Optical contact between the scintillation crystals, the light guide and the PMT was provided by a Dow Corning Q2-3067 optical couplant. The light guide was wrapped with aluminised polyethylenterephthalat film. The detector was surrounded by a passive shield made of high-purity oxygen free high conductivity (OFHC) copper (5–12 cm thickness), and lead (5 cm thickness). The data acquisition set-up based on the 12-bit, 20 MS/s transient digitizer (described in Section 3.2) was used in the measurements. The energy scale and the resolution of the detectors were determined in a calibration run with a ^{207}Bi γ-ray source.

The energy spectra of the $MgWO_4$ crystal accumulated over 17 h in the low-background set-up, using the pulse-shape discrimination technique, are presented in Fig. 14. There is a clear peak in the α-spectrum that can be assigned to ^{210}Po (daughter of ^{210}Pb and a member of the ^{238}U family). The area of the peak (291 ± 23 counts) corresponds to an activity of ^{210}Po in the crystal of 5.7 ± 0.4 Bq kg^{-1}. The equilibrium of the ^{238}U chain is broken in the crystal and hence we observed no α-peaks of the ^{226}Ra daughters: ^{218}Po ($E_\alpha \approx 6.00$ MeV) and ^{214}Po ($E_\alpha \approx 7.69$ MeV), expected above an energy of 1.25 MeV in the γ-scale. This allows us to set a limit on the activity of ^{226}Ra in the crystal of <0.05 Bq kg^{-1}. Similarly a limit can be obtained for the ^{228}Th activity in the sample, which would produce α-events with energies above 1.25 MeV from decays of ^{220}Rn ($E_\alpha \approx 6.29$ MeV) and ^{216}Po ($E_\alpha \approx 6.78$ MeV).

An α-peak might be expected from the internal contamination of the detector by ^{147}Sm ($E_\alpha \approx 2.25$ MeV). To test for the presence of ^{147}Sm, the spectrum was fitted by a simple model consisting of a Gaussian function with FWHM = 28% to describe the expected α-peak of ^{147}Sm (we applied the square root dependence of the energy resolution on the energy of the α-particles), and a first-order polynomial function to describe background. Typically, the α/β ratio increases with the energy of the α-particles above 2 MeV (see, e. g., [31,32,38]). As we do not know the exact α/β ratio for ^{147}Sm, the assumed position of the expected peak was varied with the step of 10 keV within the energy range of 300–400 keV in the γ-scale. The fit of the α-spectrum by the model in the energy interval 150–650 keV gives limits on the area of the ^{147}Sm peak in the range 11–27 counts, which can be excluded with 90% confidence level (C.L.). From the maximal value, one can calculate a limit on the activity of ^{147}Sm of <0.54 Bq kg^{-1}.

We can also set limits on the presence of the β-active ^{210}Bi (expected to be in equilibrium with ^{210}Pb from the ^{238}U chain), ^{40}K, and ^{90}Sr–^{90}Y in the crystal. The corresponding distributions were simulated using the GEANT4 package [39,40]. To estimate the presence of these radionuclides we used a simple and conservative approach: we expect the simulated energy

distributions not to exceed the experimental data (plus error bars) in any part of the measured spectrum. This gives a limit for the area of the ^{210}Bi distribution of 120 counts (90% C.L.) (see Fig. 14b). This corresponds to a limit on the ^{210}Pb internal contamination of $<2.4\,\mathrm{Bq\,kg^{-1}}$. In the same way limits on radioactive contamination by ^{40}K and ^{90}Sr–^{90}Y were obtained. A summary of the measured radioactive contamination of the $MgWO_4$ crystal scintillator (or limits on their activities) is given in Table 3.

Apparently, ^{210}Po is the dominant constituent of the intrinsic radioactive background of $MgWO_4$, but currently we cannot give an unambiguous explanation for this observation. Interestingly, $ZnWO_4$ crystal scintillators grown from the same batch of WO_3 exhibit extremely low radioactive background: in particular, it exhibits a ^{210}Po contamination that does not exceed $0.2\,\mathrm{mBq\,kg^{-1}}$ [27,41]. Both materials were produced at the same facility. This fact indicates that the radioactive contamination conceivably is brought to the crystal by other ingredients used in the crystal growth: either MgO or the Na_2WO_4 flux. Of these two, sodium tungstate has the lowest purity and hence is the most likely cause of the problem. Nevertheless, to answer this question we are planning to carry out an extensive examination of the raw materials using α and γ-spectroscopy and to measure a crystal of larger volume to improve the sensitivity of the low-background measurements.

4. Conclusions

We have developed a technique for the growing $MgWO_4$ crystals by pulling a seed from the melted flux solution, and used this to produce $\approx 1\,\mathrm{cm^3}$ crystals of good optical quality. The optical and scintillation properties of this new crystal scintillator were systematically studied for the first time. Though reasonably transparent, the crystal exhibits noticeable absorption at 320–420 nm due to the presence of impurities and/or defects. The crystal shows a broad emission band with a maximum at 470 nm under X-ray excitation. The afterglow of the crystal is found to be 0.035% 20 ms after termination of X-ray excitation.

The relative photoelectron output was evaluated using 80 μs records of the scintillation signal, and found to be 35% that of $CdWO_4$ and 27% that of NaI(Tl). As this is the first single $MgWO_4$ crystal produced, this is merely a benchmark value and we anticipate the optimisation of the crystal production process will lead to a substantial improvement of these parameters, in particular the transparency [42]. The energy resolution of a small (≈ 0.9 g) sample $MgWO_4$ crystal scintillator was measured for X-ray and γ-quanta excitation in the energy interval 17–1064 keV, giving 9.1% for the 662 keV γ-quanta of ^{137}Cs. We have found that $MgWO_4$ exhibits a non-proportionality of the scintillation response that is typical for oxide scintillators: the light output decreases for low-energy γ-quanta.

The response to α-particles was investigated with a collimated ^{241}Am source. Similar to other tungstates, i.e. $ZnWO_4$ and $CdWO_4$, the quenching of α-particles in $MgWO_4$ depends on the direction of the irradiation; this results in the variation of the α/β ratio in the range 0.16–0.19.

The pulse shape of scintillation signals for γ-quanta and α-particles was investigated. Four decay components were observed with $\tau_i \approx 0.1$–0.2 μs, 1–2 μs, ≈7–10 μs, and ≈30–40 μs at room temperature, depending on the type of excitation. We have demonstrated that the difference in the scintillation pulse shape can be used to discriminate α-particles and γ-quanta.

The relative intensity and scintillation decay kinetics were investigated over the temperature range 7–305 K. The relative scintillation efficiency of $MgWO_4$ is found to be $33 \pm 12\%$ that of $ZnWO_4$ at $T = 7$ K.

Measurements of the intrinsic radioactivity in a low-background set-up showed that the $MgWO_4$ crystal is contaminated with ^{210}Po at a level of $5.7 \pm 0.4\,\mathrm{Bq\,kg^{-1}}$. Contamination by other active nuclides from the U/Th chains was estimated to be $<0.05\,\mathrm{Bq\,kg^{-1}}$ (^{226}Ra and ^{228}Th)$< 0.28\,\mathrm{Bq\,kg^{-1}}$ (^{232}Th) and $<2.4\,\mathrm{Bq\,kg^{-1}}$ (^{210}Pb). The activity of ^{40}K, ^{90}Sr–^{90}Y and ^{147}Sm does not exceed 1.6, 1.5 and $0.54\,\mathrm{Bq\,kg^{-1}}$, respectively.

Altogether these results demonstrate that $MgWO_4$ has a good prospect as a scintillation detector for particular applications, such as rare event searches that require a range of different cryogenic scintillators. Therefore the development and optimisation of the technology to produce large $MgWO_4$ crystal scintillators with improved performance characteristics and low intrinsic radioactive background is currently in progress at the Institute for Scintillation Materials.

Acknowledgments

The authors are very grateful to Dr. V.N. Baumer (Institute for Single Crystals, Kharkiv, Ukraine) for the orientation of the $MgWO_4$ crystal. We would like to thank Dr. V.V. Kobychev (Institute for Nuclear Research, Kyiv, Ukraine) for Monte Carlo simulation of the background components. The study was supported in part by a grant from the Royal Society (London) "Development of advanced scintillation detectors for cryogenic dark matter search". The support of the group from the Institute for Nuclear Research (Kyiv, Ukraine) by the project "Kosmomikrofizyka" (Astroparticle Physics) of the National Academy of Sciences of Ukraine is gratefully acknowledged.

References

[1] P. Meunier, et al., Appl. Phys. Lett. 75 (1999) 1335.
[2] G. Angloher, et al., Astropart. Phys. 31 (2009) 270.
[3] S. Pirro, C. Arnaboldi, J.W. Beeman, G. Pessina, Nucl. Instr. and Meth. A 559 (2006) 361.
[4] C. Cozzini, et al., Phys. Rev. C 70 (2004) 064606.
[5] H. Kraus, et al., J. Phys.: Conf. Ser. 39 (2006) 139.
[6] V.B. Mikhailik, H. Kraus, J. Phys. D: Appl. Phys. 39 (2006) 1181.
[7] V.B. Mikhailik, et al., J. Phys.: Condens. Matter 20 (2008) 365219.
[8] G. Blasse, B.C. Grabmaier, Luminescent Materials, Springer, Berlin, Heidelberg, 1994.
[9] L.L. Nagornaya, et al., IEEE Nucl. Sci. Symp. Conf. Rec. N55–7 (2008) 3266 (accepted to IEEE Trans. Nucl. Sci.).
[10] L.N. Lymarenko, et al., Effect of Structural Defects on Physical Properties of Tungstates, Vyshcha Shkola, Lviv, 1978, p. 160.
[11] Luke L.Y. Chang, et al., J. Am. Ceram. Soc. T-7 (1966) 385.
[12] J. Macavei, H. Schulz, Z. Kristallogr. 207 (1993) 193.
[13] John R. Günter, et al., Solid State Ion. 32/33 (1989) 141.
[14] J.P. Chu, et al., Mater. Chem. Phys. 53 (1998) 172.
[15] E. Broch, Z. Phys. Chem. B 1 (1928) 409.
[16] E.K. Broch, Untersuchungen über Kristallstrukturen des Wolframthypus und des Scheelitthypus, Norsk. Acad., Oslo, Mat.-Nat., K1 8, 1929.
[17] O.S. Filipenko, et al., Kristallografiya 13 (1968) 1073; Sov. Phys. Crystallogr. 13 (1968) 933.
[18] V.B. Kravchenko, Zh. Strukt. Khim. 10 (1969) 148.
[19] A.W. Sleight, Acta Crystallogr. B 28 (1972) 2899.
[20] A.N. Otte, et al., Nucl. Instr. and Meth. A 545 (2005) 705.
[21] http://www.detectors.saint-gobain.com/.
[22] http://www.photonis.com.
[23] P. Dorenbos, J.T.M. de Haas, C.W.E. Van Eijk, Radiat. Meas. 24 (1995) 355.
[24] M. Moszynski, et al., IEEE Trans. Nucl. Sci. NS-52 (2005) 3124.
[25] L. Bardelli, et al., Nucl. Instr.and Meth. A 569 (2006) 743.
[26] M. Moszyński, et al., Nucl. Instr.and Meth. A 553 (2005) 578.
[27] H. Kraus, et al., Nucl. Instr. and Meth. A 600 (2009) 594.
[28] E.P. Sysoeva, O.V. Zelenskaya, E.V. Sysoeva, IEEE Trans. Nucl. Sci. NS-43 (1996) 1282.
[29] M. Balcerzyc, et al., IEEE Trans. Nucl. Sci. NS-47 (2000) 1319.
[30] B.D. Rooney, J.D. Valentine, IEEE Trans. Nucl. Sci. NS-44 (1997) 509.
[31] F.A. Danevich, et al., Phys. Rev. C 67 (2003) 014310.
[32] F.A. Danevich, et al., Nucl. Instr. and Meth. A 544 (2005) 553.
[33] E. Gatti, F. de Martini, in: Nuclear Electronics 2, IAEA, Vienna, 1962, p. 265.
[34] T. Fazzini, et al., Nucl. Instr. and Meth. A 410 (1998) 213.

[35] H. Kraus, V.B. Mikhailik, D. Wahl, Nucl. Instr. and Meth. A 553 (2005) 522.
[36] G. Blasse, Structure and Bonding 42 (1980) 1.
[37] V.B. Mikhailik, et al., Phys. Rev. B 75 (2007) 184308.
[38] Yu.G. Zdesenko, et al., Nucl. Instr. and Meth. A 538 (2005) 657.
[39] S. Agostinelli, et al., Nucl. Instr. and Meth. A 506 (2003) 250.
[40] J. Allison, et al., IEEE Trans. Nucl. Sci. NS-53 (2006) 270.
[41] P. Belli, et al., Nucl. Phys. A 826 (2009) 256.
[42] F. Danevich, et al., Phys. Stat. Sol. A 205 (2007) 335.